Proceedings of the 28th IEEE
EMBS Annual International Conference
New York City, USA, Aug 30-Sept 3, 2006

Software Phantom for the Synthesis of Equilibrium Radionuclide Ventriculography Images

Oscar Ruiz-de-Jesus, Oscar Yanez-Suarez, Luis Jimenez-Angeles, and Enrique Vallejo-Venegas

***Abstract*— This paper presents the novel design of a software phantom for the evaluation of equilibrium radionuclide ventriculography systems. Through singular value decomposition, the data matrix corresponding to an equilibrium image series is decomposed into both spatial and temporal fundamental components that can be parametrized. This parametric model allows for the application of user-controlled conditions related to a desired dynamic behavior. Being invertible, the decomposition is used to regenerate the radionuclide image series, which is then translated into a DICOM ventriculography file that can be read by commercial equipment.**

I. Introduction

Gated equilibrium radionuclide ventriculography (ERV) is a nuclear imaging technique which provides indirect knowledge of the cardiac pumping action, allowing the evaluation of atrial-ventricular synchronicity patterns or the ejection fraction (EF). These parameters of cardiac function have relevant diagnostic and prognostic value in medicine.

Functional images obtained from this kind of study provide dynamical physiological information, beyond the purely anatomical or structural representation of the beating heart. The acquisition of an ERV series is gated by the electrocardiographic signal, establishing a temporal relation between image formation and ventricular contraction events throughout a cardiac cycle [1].

An ERV study comprises a series of K images, each one corresponding to a K-th portion of a cardiac cycle. Average pixel intensity change within a given region of interest (ROI), across the K images, generates a time series which represents the tissue or cavity behavior in that particular zone. Quantification of atrial-ventricular, intra- and inter-ventricular contraction synchronicities results from the mathematical analysis of these time series along the relevant ROIs.

Diverse quantitative parameters are generated from different alternatives of ERV analysis schemes. Distortion of these parameters occurs due to inadequate modelling, inaccurate definition of ROIs, or geometric factors due to the acquisition technique and/or anatomical constraints [2]. Therefore, technical limitations arise, as there is no reference gold standard for evaluation of ERV analysis tools (although some costly and limited mechanical models do exist [2],[3],[4],[5]). In this perspective, a software phantom could be a reasonable choice, if it could synthesize an ERV series out of controlled dynamical parameter specifications that could be verified with a given analysis tool. Such a phantom is developed in the present work.

O. Ruiz, L. Jimenez, and O. Yanez are with the Neuroimaging Laboratory, Department of Electrical Engineering, Universidad Autonoma Metroplitana - Iztapalapa, Mexico. email: cbi204280078@xanum.uam.mx, jimlui@gmail.com, yaso@xanum.uam.mx

E. Vallejo is with the Department of Nuclear Cardiology, National Institute of Cardiology, Mexico. email: epvv2@hotmail.com

II. Temporal-Spatial Decomposition of the ERV Data Matrix

An ERV image series consists of K images $I_k[n,m]$ of size $N \times M$ pixels, each one corresponding to a spatially ordered representation of the measured activities at location (n,m) of the discrete field of view at instant k, with $0 \leq k < K$. For a fixed (n,m) pair, a time series $c_{n,m}[k] = I_k[n,m]$ is obtained. These time series are commonly called in the literature as the *time-activity* curves (TAC) [6],[7] of the ERV. Two alternative representations of the ERV image series can be constructed by simple reorganization of the data into *spatial-activity* and *time-activity* **vectors**, $\mathbf{s}_k$ and $\mathbf{t}_{m,n}$, respectively, as follows:

$$\mathbf{s}_k = \begin{bmatrix} I_k[0,0] \\ \vdots \\ I_k[0,M-1] \\ \vdots \\ I_k[n,m] \\ \vdots \\ I_k[N-1,0] \\ I_k[N-1,M-1] \end{bmatrix}, \quad \mathbf{t}_{n,m} = \begin{bmatrix} I_0[n,m] \\ I_1[n,m] \\ \vdots \\ I_{K-1}[n,m] \end{bmatrix} \tag{1}$$

where the spatial-activity vector $\mathbf{s}_k$ results from row-wise stacking the activities from the k-th ERV image and the time-activity vector $\mathbf{t}_{n,m}$ corresponds to the collection of activities in the time series $c_{n,m}[k]$.

Using these definitions, the ERV image series can be represented as either a *temporal data matrix* $\mathbf{T}$

$$\mathbf{T} = \begin{bmatrix} \mathbf{t}_{0,0} & \cdots & \mathbf{t}_{0,M-1} & \cdots \\ & & & \mathbf{t}_{N-1,0} \quad \cdots \quad \mathbf{t}_{N-1,M-1} \end{bmatrix}' \tag{2}$$

or a *spatial data matrix* $\mathbf{S}$

$$\mathbf{S} = \begin{bmatrix} \mathbf{s}_0 & \cdots & \mathbf{s}_{K-1} \end{bmatrix}' \tag{3}$$

where clearly $\mathbf{S} = \mathbf{T}'$.

Now, these two representations allow the straightforward estimation of the temporal and spatial correlation matrices of the ERV data:

$$\hat{\mathbf{R}_T} = \frac{1}{K}\mathbf{T}'\mathbf{T}, \quad \hat{\mathbf{R}_S} = \frac{1}{NM}\mathbf{S}'\mathbf{S} \tag{4}$$

The eigendecomposition $\hat{\mathbf{R}_T}\mathbf{V} = \mathbf{V}\mathbf{\Lambda}$ of the temporal correlation matrix is commonly used in ERV analysis from the perspective of factor analysis or PCA. On the other hand, the corresponding decomposition of the spatial correlation is rarely used, if at all [8]. Singular value decomposition (SVD) of the time-activity matrix $\mathbf{T}$

$$\mathbf{T} = \mathbf{U}\mathbf{\Sigma}\mathbf{V}' \tag{5}$$

yields both eigendecompositions simultaneously, since it is known that the unitary matrices $\mathbf{U}$ and $\mathbf{V}$ have the following properties:

$$(\mathbf{T}'\mathbf{T})\,\mathbf{V} = \mathbf{V}\mathbf{\Lambda} \tag{6}$$

$$(\mathbf{T}\mathbf{T}')\,\mathbf{U} = (\mathbf{S}'\mathbf{S})\,\mathbf{U} = \mathbf{U}\mathbf{\Lambda} \tag{7}$$

Thus, the ERV image series, when expressed as a time-activity matrix, can be rewritten as a linear combination of spatio-temporal outer products of the spatial eigenvectors $\mathbf{u}_k$ and the temporal eigenvectors $\mathbf{v}_k$

$$\mathbf{T} = \sum_{k=0}^{K-1} \sigma_k \mathbf{u}_k \mathbf{v}_k' \tag{8}$$

where σ_k are the singular values of $\mathbf{T}$, that is, the square roots of the eigenvalues of either correlation matrix. Usually truncating the linear combination (8) yields reasonable approximations of the original data. For the case of ERV image series, the use of two components is typically enough for acceptable reconstruction [6]. This in turn means that the construction of models for the parameter set

$$\{\mathbf{u}_0, \mathbf{u}_1, \mathbf{v}_0, \mathbf{v}_1\} \tag{9}$$

represents a possible means of synthesizing ERV studies from controlled conditions, that is, a possibility of building a software-based ERV phantom. This approach is detailed in the following section.

III. Modelling the Temporal Components

A typical ventricular TAC, showing the relevant parameters such as ejection fraction, time of end-systole (TES) and peak ejection and filling rates (PER and PFR) is shown in Fig. 1 [9],[10]. In particular, the EF is determined at the sample ($k = k_{min}$, corresponding to TES) where the TAC attains its minimum value.

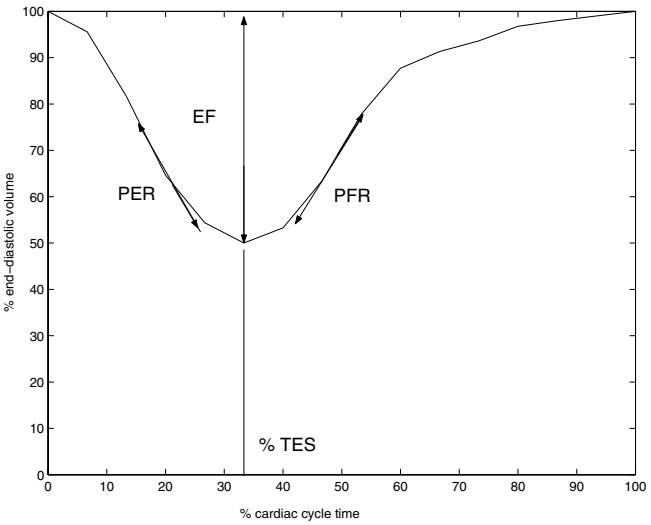

Fig. 1. Ventricular time-activity curve: EF is the ejection fraction, TES is the time of end systole, and PER and PFR are peak ejection and filling rates, respectively.

Some authors have modelled this curve as an approximation to a cosine [11],[12], while the atrial TAC is modelled by an out-of-phase cosine, 180^o delayed with respect to the ventricular TAC. In reality, these curves are far from symmetrical. To overcome this limitation in constructing the generating model, reference ventricular ($\mathbf{r}_v$) and atrial ($\mathbf{r}_a$) TACs are computed by averaging curves obtained through SVD decompositions from a set of 25 real ERVs and normalizing them in time and amplitude to fit the $[0, 1]$ interval. Interpolated versions of these vectors, $\mathbf{r}_{vi}$ and $\mathbf{r}_{ai}$, respectively, are obtained performing cubic splines interpolation to the desired temporal resolution.

The $\mathbf{r}_{vi}$ time-activity vector is used in the ventricular TAC model of Kerleau *et al* [10], to construct the first temporal component $\mathbf{v}_0$ (see (9)) with desired EF and TES parameters:

$$\mathbf{v}_0\,[k] = \mathbf{r}_{vi}\left[Q\,(k)^{TES}\right]^{\beta} \tag{10}$$

where

$$\beta = \frac{log(1 - EF)}{log(\mathbf{r}_{vi,min})} \tag{11}$$

serves to scale the curve amplitude. Note that the value of $\mathbf{r}_{vi,min}$ is fixed after interpolating the average TAC and that EF is user-dependent.

Function $Q\,(k)$ is required to introduce temporal distortion so that $\mathbf{v}_0$ meets the desired end-systolic parameter. It computes the sample locations in the interpolated reference such that:

$$\sum_{k=0}^{K-1}\left(\mathbf{r}_{vi}\left[Q\,(k)\right]^{\beta} - \mathbf{r}_v\,[k]\right)^2 \tag{12}$$

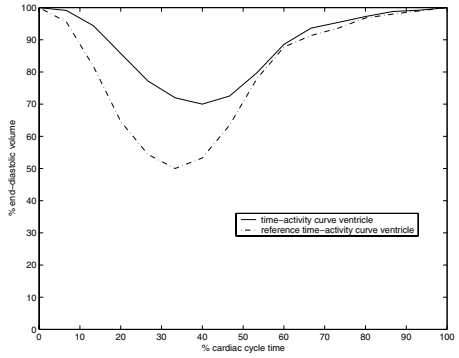

Fig. 2. Reference ventricular TAC (EF 50% TES 33%) $\mathbf{r}_{vi}$ and transformed ventricular TAC (EF 30% TES 39%) $\mathbf{v}_0$.

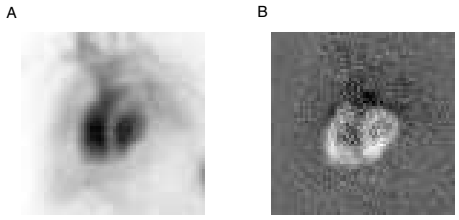

Fig. 3. (A) first spatial component, $\mathbf{u}_0$; (B) second spatial component, $\mathbf{u}_1$.

is minimized (in the least-squares sense) [10]. As an example, a simulated $\mathbf{v}_0$ temporal component with 30% EF and 39% TES is shown in Fig. 2, related to the reference vector $\mathbf{r}_{vi}$. An analogous procedure is performed to synthesize the second temporal component, $\mathbf{v}_1$.

It is mandatory for SVD reconstruction to guarantee that the temporal components $\mathbf{v}_0$ and $\mathbf{v}_1$ end up forming an orthogonal basis. In order to achieve this condition, the vectors are further processed with a Gram-Schmidt orthogonalization:

$$\mathbf{v}_{0m} = \mathbf{v}_0 \tag{13}$$

$$\mathbf{v}_{1m} = \mathbf{v}_1 - \frac{(\mathbf{v}_1' \mathbf{v}_{0m})}{\|\mathbf{v}_{0m}\|^2} \mathbf{v}_{0m} \tag{14}$$

IV. Modelling the Spatial Components

Spatial components $\mathbf{u}_0$ and $\mathbf{u}_1$ can be reshaped into two eigenimages as can be seen in Fig. 3. Spatial component $\mathbf{u}_0$ is related to the pixelwise time average counts for the ERV series and spatial component $\mathbf{u}_1$ is in turn related to the pixelwise difference between the end-diastole and the end-systole frames.

On the simulation side, the first spatial component, $\mathbf{u}_0$ is built by introducing four circles that represent each of the four cardiac cavities, within which four other circles of higher intensity are positioned. This synthetic scene is then smoothed with a Gaussian filter [13]. The simulated version

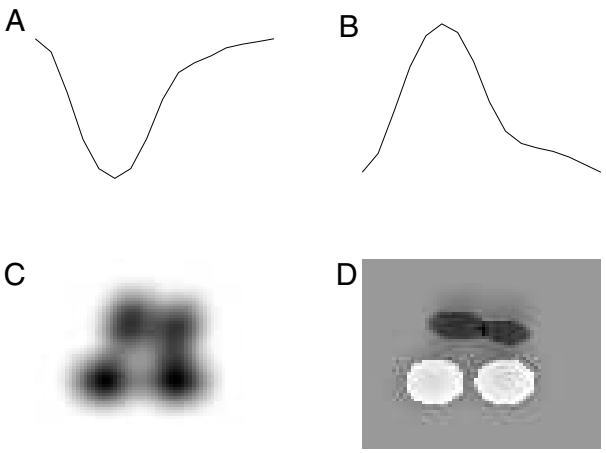

Fig. 4. (A) first temporal component, $\mathbf{v}_{0m}$; (B) second temporal component, $\mathbf{v}_{1m}$; (C) first spatial component, $\mathbf{u}_{0m}$; and (D) second spatial component $\mathbf{u}_{1m}$.

of the second spatial component, $\mathbf{u}_1$ is also modeled with the four circle basic scene, but the intensities are made positive in the ventricular positions and negative in the atrial positions.

Again, to guarantee that the spatial components form an orthogonal basis before SVD reconstruction, these vectors are transformed into the pair $\mathbf{u}_{0m}$ and $\mathbf{u}_{1m}$ by means of a Gram-Scmidt orthogonalization procedure as described before.

V. Generation of the ERV Image Series

An example of the four synthetic spatial-temporal components of the model, namely

$$\{\mathbf{u}_{0m}, \mathbf{u}_{1m}, \mathbf{v}_{0m}, \mathbf{v}_{1m}\} \tag{15}$$

is shown in Fig. 4. With them, the synthetic ERV series is constructed using inverse SVD as:

$$\mathbf{T} = \sum_{k=0}^{1} \sigma_k \mathbf{u}_{km} \mathbf{v}_{km}' \tag{16}$$

where the synthetic σ's are also generated from averaged real ERV measurements. Fig. 6 shows a software phantom simulation with dynamic parameters of 30% EF and ventricular TES of 39%, as generated with equation (16). Images are the reordered columns of T, contaminated with white Gaussian noise of standard deviation equal to 25% of the maximum frame intensity.

The image sequences are stored as tagged Nuclear-Medicine DICOM files in a straightforward manner, appending a generic nuclear medicine DICOM header to the formatted data. Total processing time, from parameter definition to DICOM file generation is less than 2 s, in the case of a 64x64x16 frame sequence.

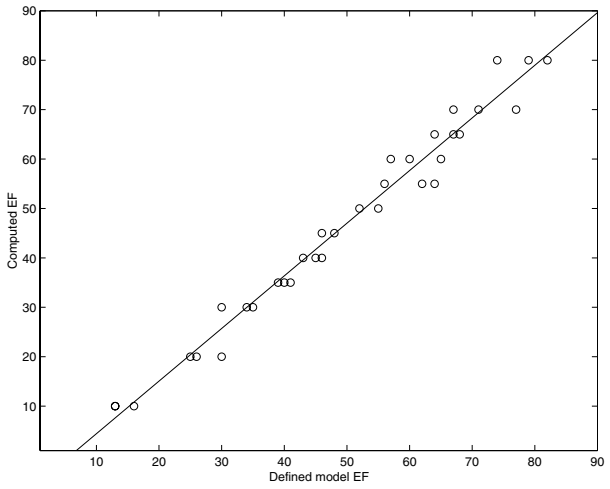

Fig. 5. Relation between modelled and computed EFs ($m = 1.07$, $b = -6.24$, $R^2 = 0.97$), as determined by standard phase analysis from the MPR/MPS system.

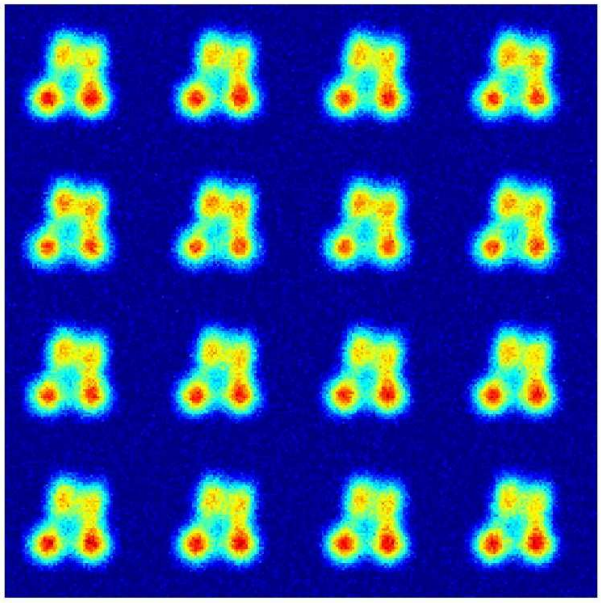

Fig. 6. Synthetic ERV series generated with the proposed model. Dynamic parameters are EF 30% and TES 39%.

VI. Model Evaluation

For the purpose of evaluating the adequacy of the model, 36 simulated ERV series were synthesised, with varying EF values. DICOM studies were then fed to a Millenium MPR/MPS (General Electric) system running the EF Analysis/Entegra (General Electric) tools for ERV phase analysis. Fig. 5 shows the linear correlation obtained between the modelled and computed fractions ($R^2 = 0.9748$).

VII. Conclusions

The design of a software phantom based on a linear combination of spatio-temporal components has been presented. These components facilitate the synthesis of ERV image series under controlled conditions like the definition of dynamic parameters such as EF or TES. While the model considers only two curves from each domain to re-synthesize an ERV series, extensions to more components can be easily derived. For example, the use of a third temporal component could incorporate synchronicity abnormalities among the ventricles. Also, the use of Gaussian profiles in the second spatial component would allow the modification of the net left ventricular volume, possibly facilitating the simulation of an infarction of ventricular walls.

VIII. Acknowledgements

This work was supported in part by the National Council of Science and Technology, through a graduate scholarship for Mr. Ruiz de Jesus, 186737.

References

[1] K. Williams, "A historical perspective on measurement of ventricular function with scintigraphic tecniques: Part II- ventricular function with gated techniques for blood pool and perfusion imaging," *Journal of Nuclear Cardiology*, vol. 12, pp. 208–215, 2005.

[2] V. Ullmann and J. Kuba, "A general purpose dynamic phantom for modelling cardiac action in radionuclide ventriculography and angiocardiography," *Physics in Medicine and Biology*, vol. 31, pp. 669–675, 1986.

[3] M. Kupinski, J. Hoppin, J. Krasnow, S. Dahlberg, J. Leppo, E. C. M.A. King, and H. Barrett, "Comparing cardiac ejection fraction estimation algorithms without a gold standard," *Academic Radiology*, vol. 13, pp. 329–337, 2006.

[4] M. Kupinski, J. Hoppin, E. Clarkson, H. Barrett, and G. Kastis, "Estimation in medical imaging without a gold standard," *Academic Radiology*, vol. 9, pp. 290–297, 2002.

[5] P. de Bondt, O. de Winter, S. Vandenberghe, F. Vandevijver, P. Segers, A. Bleukx, H. Ham, P. Verdonck, and R. A. Dierckx, "Accuracy of commercially available processing algorithms for planar ventriculography using data for a dynamic left ventricular phantom," *Nuclear Medicine Communications*, vol. 25, pp. 1197–1202, 2004.

[6] P. Hannequin, J. Liehn, and J. Valeyre, "The determination of the number of statistically significant factors in factor analysis of dynamic structures," *Physics in Medicine and Biology*, vol. 34, no. 9, pp. 1213–1227, 1989.

[7] A. Boudraa, J. Champier, M. Djebali, F. Behloul, and A. Beghdadi, "Analysis of dynamic nuclear images by covariance function," *Computarized Medical Imaging and Graphics*, vol. 23, pp. 181–191, 1999.

[8] L. Comas, P. Berthout, R. Sabbah, J. Daspet, O. Blagosklonov, M. Baud, J. Verdenet, and J. Cardot, "Use of a 4-D cardiac phantom to quantify Karhunen-Loeve images applied to myocardial gated SPECT," *Computers in Cardiology*, vol. 32, pp. 431–434, 2005.

[9] H. Muntinga, F. van den Berg, H. Knol, M. Niemeyer, P. Blanksma, H. Louwes, and E. van der Wall, "Normal values and reproducibility of left ventricular filling parameters by radionuclide angiography," *International Journal of Cardiac Imaging*, vol. 13, pp. 165–171, 1997.

[10] C. de Kerleau, J. Crouzet, E. Ahronovitz, M. Rossi, and D. Mariano-Goulart, "Automatic generation of noise-free time-activity curve with gated blood-pool emission tomography using deformation of a reference curve," *IEEE Transactions on Medical Imaging*, vol. 23, no. 4, pp. 485–491, 2004.

[11] I. Bankman, *Handbook of medical imaging processing and analysis*. Academic Press, 2000, ch. Quantitative analysis of cardiac function.

[12] E. Botvinick, R. Dunn, M. Frais, W. O'Connell, D. Shosa, R. Herfkens, and M. Scheinman, "The phase image: its relationship to patterns of contraction an conduction," *Circulation*, vol. 65, pp. 551–560, 1982.

[13] A. Sitek, E. D. Bella, and G. Gullberg, "Factor analysis with a priori knowlegde-application in dynamic cardiac SPECT," *Physics in Medicine and Biology*, vol. 45, pp. 2610–2638, 2000.